

DELAY AND DOPPLER PROCESSING FOR MULTI-TARGET DETECTION WITH IEEE 802.11 OFDM SIGNALING

Duy H. N. Nguyen¹ and Robert W. Heath Jr.²

¹ Department of Electrical and Computer Engineering, San Diego State University, San Diego, CA 92182

² Wireless Networking and Communications Group, The University of Texas at Austin, TX, USA, 78712

Email: duy.nguyen@sdsu.edu, rheath@utexas.edu

ABSTRACT

This paper investigates the processing of delay and Doppler information with IEEE 802.11p OFDM signaling for multi-target detection. We study the feasibility of extending IEEE 802.11p short-range communication (DSRC) in vehicles to automotive radio detection and ranging (radar) functionality. By exploiting the unique structure of 802.11p OFDM packets over multiple subcarriers and multiple time-slots, we apply the estimation of signal parameters via rotational invariance technique (ESPRIT) for concurrent multi-target detection and range/velocity estimation. Numerical results show sub-0.2 m accuracy in range estimation and sub-0.02 m/s accuracy in velocity estimation with high probability.

Index Terms— Radar, OFDM, 802.11, multi-target detection

1. INTRODUCTION

A recent report from the National Transportation Safety Board (NTSB) mandates the implementation of frontal collision detection and avoidance systems on all new vehicles for transportation safety [1]. This requirement can be addressed primarily through forward-facing radar [1] or dedicated short-range communication (DSRC) [2], i.e., IEEE 802.11p. Current automotive radars, such as DRW automatic cruise control (ACC) or Delphi ACC, require hundreds of MHz in bandwidth. Thus, they have to operate at millimeter wave (mmWave) spectrum (~ 77 GHz) where large open bandwidth is available [3,4]. Unfortunately, complex antenna and hardware design with high cost may limit the market penetration of these mmWave radars.

Successful integration of DSRC with radar functionality can provide substantial opportunities for automotive radar at low cost. There has been significant research on passive radar with 802.11 waveform [5–8]. Active radar technology with 802.11 packets have been investigated as well but received less attention in [9, 10]. IEEE 802.11p waveforms, which only operate with 10 MHz spectrum at 5.89 GHz, might not provide sufficient resolution for automotive applications. In [11], an exhaustive search method was proposed to obtain sub-1 m ranging accuracy for a single target using 802.11p. This result was already an improvement to the OFDM radar studied in [12–14], where the range resolution of 1.61 m and the velocity resolution of 1.97 m/s were achieved with 91.1 MHz of signal bandwidth at radar carrier frequency of 24 GHz [14].

In this work, we examine algorithmic signal processing techniques for delay and Doppler information with IEEE 802.11p OFDM

This material is based upon work supported in part by the National Science Foundation under Grant No. NSF-1549663, by the U.S. Department of Transportation through the Data-Supported Transportation Operations and Planning (D-STOP) Tier 1 University Transportation Center, and by the SDSU University Grants Program.

signaling. We first show that periodogram-based methods used in [14] does not provide sufficient range/velocity resolution with 802.11p. We then study the application of the estimation of signal parameters via rotational invariance technique (ESPRIT) for processing 802.11p packets. Numerical results show sub-0.2 m accuracy in range estimation and sub-0.02 m/s accuracy in velocity estimation using only few measurements across multiple subcarriers and time-slots.

2. MODELING RADAR SIGNALS WITH DELAY AND DOPPLER EFFECTS

We consider a monostatic radar configuration with one transmit and one receive antenna. The wireless channel between the transmitter and receiver can be modeled as a multipath channel, where each path represents the round-trip reflection from a target. The multipath baseband equivalent of a radar channel then can be written as [15]

$$h_b(\tau, t) = \sum_i a_i(t) e^{-j2\pi f_c \tau_i(t)} \delta(\tau - \tau_i(t)) \quad (1)$$

where $\tau_i(t)$ is the reflected signal delay from target i , $a_i(t) e^{-j2\pi f_c \tau_i(t)}$ is the baseband time-varying gain of the reflected signal from target i , and f_c is the carrier frequency. We assume that the magnitude of channel gain $a_i(t)$ follows the radar equation [16] and thus depends on the instantaneous target i 's range. Similarly, the time-varying delay $\tau_i(t)$ is modeled accordingly to the range of target i such that

$$\tau_i(t) = \tau_i^o + 2tv_i/c \quad (2)$$

where $\tau_i^o = 2d_i^o/c$ is the initial delay, d_i^o is the initial range and v_i is the relative velocity between the target i and the radar. Herein, $v_i > 0$ (or $v_i < 0$) indicates that the target is moving away (or towards) the radar.

By taking the Fourier transform of (1), we obtain the baseband frequency response for frequency f at a given time t :

$$\begin{aligned} H_b(f, t) &= \int_{-\infty}^{\infty} h_b(\tau, t) e^{-j2\pi f \tau} d\tau \\ &= \sum_i a_i(t) e^{-j2\pi(f+f_c)\tau_i(t)} \\ &= \sum_i a_i(t) e^{-j2\pi f_c \tau_i^o} e^{-j2\pi f \tau_i^o} e^{-j4\pi(f_c+f)tv_i/c}. \end{aligned} \quad (3)$$

With OFDM in current IEEE 802.11 standards, frequency-domain channel estimations enabled by discrete Fourier transform (DFT) are typically provided. Assuming perfect synchronization, perfect band-limited signals, perfect estimation algorithms, we take the samples of the baseband frequency response at frequency spacing (subcarrier

bandwidth) Δ_f and time spacing (sampling interval) Δ_t . With K targets, the baseband frequency response at subcarrier m and time-slot n is given by

$$\begin{aligned} H_b[m, n] &= a_0 e^{-j\theta_0} + \sum_{i=1}^K a_i[n] e^{-j2\pi f_c \tau_i^\circ} e^{-j2\pi \tau_i^\circ \Delta_f m} \\ &\quad \times e^{-j4\pi(f_c + \Delta_f m)(v_i/c)\Delta_t n} \\ &= a_0 e^{-j\theta_0} + \sum_{i=1}^K a_i[n] e^{-j\theta_i} e^{-j\kappa_i m} e^{-j\nu_i n} e^{-j\varepsilon_i m n} \end{aligned} \quad (4)$$

where a_0 is the time-invariant and frequency-invariant response due to the direct path between the radar's transmit and receive antennas, θ_0 is the constant phase shift of the direct path. For ease of presentation, we replace $\kappa_i = 2\pi\tau_i^\circ\Delta_f = (4\pi d_i^\circ/c)\Delta_f$, $\nu_i = (4\pi f_c v_i/c)\Delta_t$, $\varepsilon_i = (4\pi v_i/c)\Delta_f\Delta_t$ and $\theta_i = 2\pi f_c \tau_i^\circ$. Note that $\varepsilon_i \ll \kappa_i$ and $\varepsilon_i \ll \nu_i$.

3. SYSTEM PARAMETERIZATION

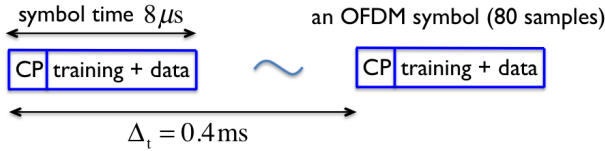


Fig. 1. Parameterizing 802.11 OFDM signaling for radar operation.

In Fig. 1, we illustrate the structure of IEEE 802.11 OFDM signaling that is used for radar operations. The 802.11 OFDM signaling is assumed to have $B = 10$ MHz bandwidth with 64 subcarriers. The sampling time is $T = 1/B = 0.1 \mu\text{s}$. Each OFDM symbol contains 16 samples for cyclic prefix (CP) and 64 samples for training and data. Of 64 subcarriers in 802.11, 48 are used for data transmission, 4 are used for training, and 12 are zeroed to reduce adjacent channel interference. Thus, we use the measurements obtained from 52 useful subcarriers in each OFDM symbol for radar functionality. We then take the measurements every 50 OFDM symbols, *i.e.*, $\Delta_t = 0.4$ ms, for Doppler processing. The setting of Δ_t , which has a profound effect on velocity estimation, will be explained shortly.

3.1. Ambiguity

3.1.1. Range Ambiguity

The baseband frequency response (1) over N subcarriers at a given time-slot \bar{n} can be organized into

$$\begin{aligned} H_b[m, \bar{n}] &= a_0 e^{-j\theta_0} + \sum_{i=1}^K a_i[\bar{n}] e^{-j\theta_i} e^{-j\nu_i \bar{n}} e^{-j(\kappa_i + \bar{n}\varepsilon_i)m}, \\ &\quad m = 1, \dots, N. \end{aligned} \quad (5)$$

From (5), $H_b[m, \bar{n}]$ is the summation of complex-valued sinusoidal signals at angular frequencies $-(\kappa_i + \bar{n}\varepsilon_i)$. Since $\kappa_i + \bar{n}\varepsilon_i = (4\pi\Delta_f/c)(d_i^\circ + \Delta_t\bar{n}v_i)$, the range of target i at time-slot \bar{n} can be deduced from the estimation of the frequency $\kappa_i + \bar{n}\varepsilon_i$.

To detect an arbitrary target i at range $d_i[\bar{n}] \triangleq d_i^\circ + \Delta_t\bar{n}v_i$ without ambiguity, $\kappa_i + \bar{n}\varepsilon_i$ must comply

$$0 \leq \kappa_i + \bar{n}\varepsilon_i \leq 2\pi \quad \Rightarrow \quad d_i[\bar{n}] \leq \frac{c}{2\Delta_f} = \frac{cN}{2B} \quad (6)$$

where B is the spectrum bandwidth. Since the signal delay must be nonnegative, the unambiguous range interval is defined as $[0, 2\pi]$.

Effectively, the detection range without ambiguity depends on the subcarrier spacing Δ_f . For a IEEE 802.11p signal with 10 MHz of bandwidth divided into 64 subcarriers, the detection range is 960 m, which is well above existing automotive radars on the market, such as TRW's 77 GHz ACC system and Delphi's 76 GHz ACC system.

3.1.2. Velocity Ambiguity

To detect a target using its Doppler shift, the baseband frequency response (1) is observed over $T > 1$ time-slots

$$\begin{aligned} H_b[\bar{m}, n] &= a_0 e^{-j\theta_0} + \sum_{i=1}^K a_i[n] e^{-j\theta_i} e^{-j\kappa_i \bar{m}} e^{-j(\nu_i + \bar{m}\varepsilon_i)n}, \\ &\quad n = 1, \dots, T. \end{aligned} \quad (7)$$

At a given subcarrier \bar{m} , $H_b[\bar{m}, n]$ is a summation of complex-valued sinusoid signals at angular frequencies $-(\nu_i + \bar{m}\varepsilon_i)$. Since $\nu_i + \bar{m}\varepsilon_i = (4\pi\Delta_t v_i/c)(f_c + \bar{m}\Delta_f)$, the estimation of the frequency $\nu_i + \bar{m}\varepsilon_i$ also provides the estimation of target i 's velocity. To estimate v_i without ambiguity, $\nu_i + \bar{m}\varepsilon_i$ must comply

$$-\pi \leq \nu_i + \bar{m}\varepsilon_i \leq \pi \quad \Rightarrow \quad -\frac{c}{4f_c\Delta_t} \leq v_i \leq \frac{c}{4f_c\Delta_t}. \quad (8)$$

Effectively, the maximum detection velocity depends on the carrier frequency and the sampling interval. With the carrier frequency of IEEE 802.11p at $f_c = 5.89$ GHz and a sampling interval $\Delta_t = 0.4$ ms, it is possible to detect and estimate a target's velocity within $[-32, +32]$ m/s or $[-72, +72]$ mph.

3.2. Resolution with Periodogram-based Methods

A straightforward approach to estimate the frequency of a sinusoid is to examine the power spectral density of a sample vector. However, classical periodogram-based methods, such as the DFT, are only capable of resolving spectral lines separated by more than $1/N$ cycles per sampling interval [17]. Therefore, $2\pi/N$ is the spectral resolution limit of the DFT method. In [14], the authors utilized the DFT/IDFT of the OFDM-based radar signal to compute the periodogram and estimate the target range and velocity. Under the consideration of IEEE 802.11p signaling in this paper, the same approach would resolve as follows:

- Range resolution: $\Delta d = \inf_{i \neq j} |d_i - d_j| \geq \frac{2\pi}{4\pi N \Delta_f / c} = \frac{c}{2B}$, which is dependent on the spectrum bandwidth B . With $B = 10$ MHz, the range resolution is 15 m. The closest detectable target is also at 15 m, which is clearly insufficient for automotive applications.
- Velocity resolution: $\Delta v = \inf_{i \neq j} |v_i - v_j| \geq \frac{c}{2f_c T \Delta_t}$, which is dependent on the carrier frequency and the observation time $T\Delta_t$. If the automotive radar requires information update every 50 ms, the velocity resolution will be ~ 0.25 m/s. Note that a smaller Δ_t would increase the maximum detectable velocity. However, T must be increased accordingly to maintain the same resolution.

It is observed in the above calculations that using periodogram-based methods for 802.11p signaling (10 MHz bandwidth at 5.89 GHz) will not sufficiently resolve different targets for automotive radar applications. To this end, we investigate how ESPRIT method can significantly improve the radar resolution of 802.11p signaling.

4. ESPRIT FOR TARGET DETECTION AND ESTIMATION WITH 802.11P

4.1. ESPRIT

In this section, we briefly revisit the ESPRIT method for estimation of line spectra. Line spectral estimation deals with the signals from

a sample vector of length N containing K sinusoids:

$$y[t] = x[t] + e[t]; \quad x[t] = \sum_{i=1}^K \alpha_i e^{j(\omega_i t + \theta_i)} \quad (9)$$

where $e[t]$ is the zero-mean AWGN with variance σ^2 .

Let $\tilde{\mathbf{y}}[t] = [y[t], y[t-1], \dots, y[t-L+1]]^T$ as a sample vector of length- L for some $L > K$. The covariance matrix model of the data can be readily derived as $\mathbf{R} \triangleq \mathbb{E}\{\tilde{\mathbf{y}}[t]\tilde{\mathbf{y}}^*[t]\}$, whose eigenstructure contains complete information on the frequencies ω_i 's [17]. Perform eigen-decomposition of \mathbf{R} and let $\mathbf{S} = [\mathbf{s}_1, \dots, \mathbf{s}_K]$ be the matrix containing K orthonormal eigenvectors associated with the K largest eigenvalues of \mathbf{R} . Let $\mathbf{S}_1 = [\mathbf{I}_{L-1} \quad \mathbf{0}]\mathbf{S}$ and $\mathbf{S}_2 = [\mathbf{0} \quad \mathbf{I}_{L-1}]\mathbf{S}$. The ESPRIT method estimate the frequencies ω_i as $-\angle \hat{\nu}_i$, where $\hat{\nu}_i$'s are the eigenvalues of $\hat{\phi} = (\hat{\mathbf{S}}_1^* \hat{\mathbf{S}}_1)^{-1} \hat{\mathbf{S}}_1^* \hat{\mathbf{S}}_2$ [17, 18].

Once the frequencies are estimated as $\hat{\omega}_i$, the amplitudes α_i 's and phases θ_i 's (replaced by $\beta_i = \alpha_i e^{j\theta_i}$) can be estimated by the least square method, whose closed-form solution is

$$\hat{\boldsymbol{\beta}} = (\mathbf{W}^* \mathbf{W})^{-1} \mathbf{W}^* \mathbf{y} \quad (10)$$

where

$$\mathbf{W} = \begin{bmatrix} e^{j\hat{\omega}_1 \cdot 1} & \dots & e^{j\hat{\omega}_K \cdot 1} \\ \vdots & \ddots & \vdots \\ e^{j\hat{\omega}_1 \cdot N} & \dots & e^{j\hat{\omega}_K \cdot N} \end{bmatrix}. \quad (11)$$

4.2. Range and Velocity Estimation using ESPRIT

4.2.1. Range Estimation with Reflected Signal Delays (Method I-A)

The measured channels in (5) at a given time-slot n across the N subcarriers resemble a composition of multiple frequencies at $\kappa_1, \dots, \kappa_K$ and the direct path $a_0 e^{-j\theta_0}$. At first, we assume the number of targets is known a priori. Hence, ESPRIT can be readily to estimate $\kappa_1, \dots, \kappa_K$ and the target ranges accordingly. We note that the covariance matrix \mathbf{R} has to be constructed from sample vectors of length- L , where L is set to be $K+2$ to account for all K targets and the direct path. The estimated frequency closest to 0, which corresponds to the direct path, is then discarded.

If the number of targets K is an unknown with a deterministic upper bound, the length of the sample vectors must be set higher this upper bound. The number of eigenvalues of the resulting covariance matrix \mathbf{R} whose values exceed the noise floor then indicates the number of targets. The process of estimating the target ranges follows accordingly.

4.2.2. Velocity Estimation with Doppler Frequencies (Method I-B)

The channel response at a particular subcarrier m can be measured over multiple time-slots. With T measurements, the channel response vector in (7) is a summation of multiple frequencies at ν_1, \dots, ν_K and the direct path $a_0 e^{-j\theta_0}$. Therefore, ESPRIT can be used for estimating the frequencies ν_1, \dots, ν_K and hence the velocities of the K targets. Due to the time-varying ranges of the targets, the amplitudes of the sinusoids $a_i[n]$ given in (7) may change during the observing interval $T\Delta_t$. However, it is arguably true that $a_i[n]$ remains constant with a short observing time (~ 50 ms).

4.3. Target Detection and Estimation using Phase Shifts

In the previous section, the target identification and range-velocity estimation are performed with the measurements either at one time-slot across multiple subcarriers or at one subcarrier across multiple time-slots. In this section, we look at the processing of signal measurements across multiple time-slots and multiple subcarriers.

4.3.1. Velocity Estimation using Phase Shifts (Method II-A)

The measurements at two consecutive time-slots across the N subcarriers are given by

$$\begin{aligned} H_b[m, n] &= a_0 e^{-j\theta_0} + \sum_{i=1}^K a_i[n] e^{-j\theta_i} e^{-j\nu_i n} e^{-j(\kappa_i + n\varepsilon_i)m} \\ H_b[m, n+1] &= a_0 e^{-j\theta_0} + \sum_{i=1}^K a_i[n] e^{-j\theta_i} e^{-j\nu_i(n+1)} \\ &\quad \times e^{-j(\kappa_i + (n+1)\varepsilon_i)m}, \quad m = 1, \dots, N. \end{aligned} \quad (12)$$

The phase shift between the two corresponding sinusoidal signals is of interest, since it reveals the velocity of the target. By estimating this phase shift, amounted as ν_i , it is possible to find the velocity of target i using only two time-slots.

We note that Method II-A is deployed in conjunction with Method I-A. Denote $\hat{\kappa}_i$'s as the estimated frequencies using Method I-A. The amplitudes and phases of the sinusoids can be estimated using the least square solution (10). Denote $\boldsymbol{\beta}[n] = [a_0 e^{-j\theta_0}, a_1 e^{-j\theta_1} e^{-j\nu_1 n}, \dots, a_K e^{-j\theta_K} e^{-j\nu_K n}]^T$, $\mathbf{h}_b^n = [H_b[1, n], \dots, H_b[N, n]]^T$, and $\mathbf{W}_\kappa = [\mathbf{w}_0, \dots, \mathbf{w}_K]$ where $\mathbf{w}_i = [e^{-j\hat{\kappa}_i \cdot 1}, \dots, e^{-j\hat{\kappa}_i \cdot N}]^T$. Then, we have the estimate of $\boldsymbol{\beta}[n]$ as

$$\hat{\boldsymbol{\beta}}[n] = (\mathbf{W}_\kappa^* \mathbf{W}_\kappa)^{-1} \mathbf{W}_\kappa^* \mathbf{h}_b^n. \quad (13)$$

The phase shift of sinusoidal signal i can be estimated as

$$\hat{\nu}_i = \angle \left(\frac{\hat{\beta}_i[n+1]}{\hat{\beta}_i[n]} \right), \quad i = 1, \dots, K \quad (14)$$

which would provide the estimated target velocity. Note that Method II-A requires the targets be resolved with distinctive ranges using Method I-A first. Method II-A then enables the matching (range, velocity) for each target.

4.3.2. Range Estimation using Phase Shifts (Method II-B)

We can take a similar approach to identify and estimate the targets' ranges by calculating the phase shift between the waveforms in two consecutive subcarriers. The phase shift, amounted as κ_i , between the two sinusoidal waveforms corresponding to target i can be used to estimate the target ranges. The angular frequency $\hat{\nu}_i$ can be first estimated by the ESPRIT algorithm as in Method I-B, while the amplitudes and the phases are estimated by the least square method. The phase shift $\hat{\kappa}_i$ can be estimated in a similar fashion as in (14).

It is noted that the range estimation using the estimated phase shift requires the observation of the sinusoidal signals over multiple time-slots. For instance, with $T = 128$, the observing time is approximately 50 ms. During this time interval, the range of target i has been perturbed by an amount of $T\Delta_t \nu_i$. However, the phase shift estimation using the two sinusoidal signals does not take into account this perturbation and only provides the mean of target i 's range during this interval. To yield a more accurate range estimation at the end of T time-slots, the estimated range in Method II-B should be compensated by an amount of $T\Delta_t \hat{\nu}_i / 2$.

5. SIMULATION RESULTS

This section presents numerical results to demonstrate the detection and estimation capability of automotive radar with IEEE 802.11p packets. Fig. 2 illustrates the root mean square (RMS) error in range estimation of a one target with variable radar cross section (RCS) values. The target is assumed to travel at velocity 10 m/s relatively to the radar. For stronger targets ($\sigma \geq 0.1$ m²), both methods

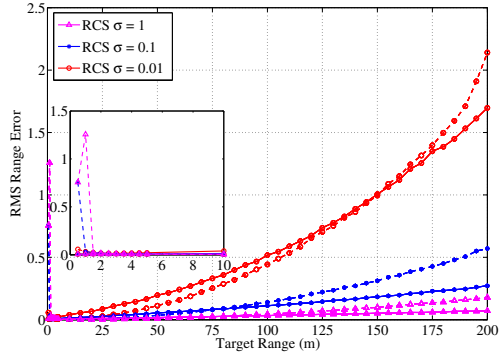


Fig. 2. RMS range error when Methods I-A and II-B are used on IEEE 802.11p packets in a 10 MHz channel with one target and variable RCS values. The target is assumed to travel at velocity 10 m/s relatively to the radar. *Solid lines* denote the results obtained from Method I-A (range estimation via signal delays) and *dashed lines* denote the results obtained from Method II-B (range estimation via phase shifts between multiple subcarriers).

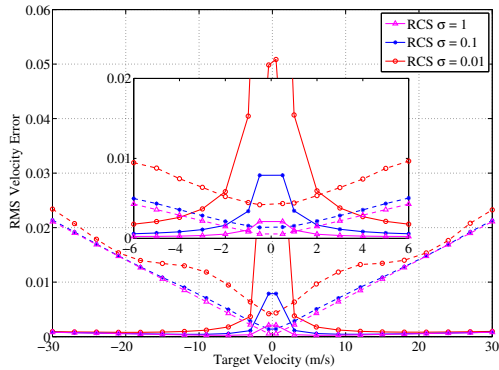


Fig. 3. RMS velocity error when Methods I-B and II-A are used on IEEE 802.11 packets using 0.4 ms sampling interval with one target and variable RCS values. The target is assumed to travel at range 30 m from the radar. *Solid lines* denote the results obtained from Method I-B (velocity estimation via Doppler shift) and *dashed lines* denote the results obtained from Method II-A (velocity estimation via phase shifts between multiple timeslots).

can obtain sub-0.2 m accuracy up to 100 m range. Method I-A can maintain sub-0.2 m accuracy up to 200 m range. For weaker targets ($\sigma = 0.01 \text{ m}^2$), both methods can obtain sub-0.5 m accuracy up to 100 m range. For targets at sub-1 m, Method I-A can provide very accurate estimation (less than 1 cm RMS error using only one time-slot measurement ($8 \mu\text{s}$)). Surprisingly, Method II-B performs very poorly for strong targets at this range. Note that Method II-B needs multiple time-slot measurements ($\sim 0.05 \text{ s}$), which might be too long for target estimation at close range.

Fig. 3 displays the root mean square (RMS) error in velocity estimation of a one target with variable RCS values. The target is assumed to travel at range 30 m from the radar. In overall, a combination of Method I-B and II-A can provide a very accurate estimation of the target velocity (RMS less than 0.005 m/s) within the velocity detection capability of the radar ($[-32, +32] \text{ m/s}$). For targets traveling at velocity greater than $\pm 4 \text{ m/s}$, Method I-B can provide the RMS less than 0.002 m/s. However, for targets traveling at smaller velocities ($[-4, +4] \text{ m/s}$ for weak targets and $[-2, +2] \text{ m/s}$

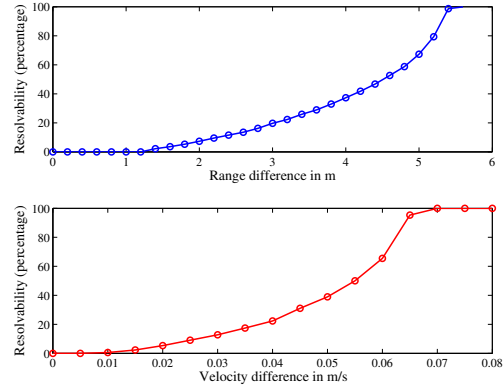


Fig. 4. The resolvability of two targets when Methods I-A and I-B are applied on IEEE 802.11 packets. The first target, located at 30 m from the radar, is traveling with velocity of 3 m/s. Subplot 1 depicts the resolvability based on the relative range difference between the two targets. The second target is also traveling with the velocity of 3 m/s. Subplot 2 depicts the resolvability based on the relative velocity difference between the two targets. The second target is at distance 30 m from the radar in this case.

for strong targets), it is more beneficial to utilize Method II-A for velocity estimation. This is because a small velocity induces a small Doppler shift to the reflected signal. Thus, the angular frequency ν_i due to the Doppler shift is also very small and becomes indistinguishable from the angular frequency at 0 due to the direct path. For weaker targets, it is even more difficult for ESPRIT to pick up the desired frequency from a much stronger DC component. In this case, it is more useful to estimate the range-rate, *i.e.*, velocity, across multiple time-slots. Method II-A allows the radar to first detect the target at its range and continuously track the phase-shift across multiple time-slots. As a result, Method II-A can estimate the range-rate, even for small velocities close to 0.

Fig. 4 illustrates the multi-target resolvability of ESPRIT-based algorithms with IEEE 802.11 packets. In these simulations, we consider the detection of two targets when their relative range is varied (with a common traveling velocity) or relative velocity is varied (with a common range from the radar). The first target, located at 30 m from the radar, is traveling with a velocity of 3 m/s. As observed in subplot 1, as the relative range between the two targets increases, the percentage of successfully resolving both targets increases. Method I-A guarantees the two-target resolvability when their relative range is above 5.4 m. Similar tendency can be observed in subplot 2 when the relative velocity between the two targets increases. Method I-B guarantees separate detections of both targets when this velocity difference is above 0.07 m/s. Finally, the results in both subplots show (at least) threefold improvements by the ESPRIT-based algorithms, compared to the periodogram-based methods.

6. CONCLUSION

This paper exploits the use of 802.11p OFDM packets for radar application. By observing the OFDM packets over multiple subcarriers and frequencies, delay and Doppler information can be extracted for ranging and velocity estimation. Numerical results show that ESPRIT can enable sub-0.2 m accuracy in range estimation and sub-0.02 m/s accuracy in velocity estimation with only 10 MHz bandwidth at 5.89 GHz. In addition, the resolvability of the radar can be improved at least threefold.

7. REFERENCES

- [1] National Transportation Safety Board, "Use of forward collision avoidance systems to prevent and mitigate rear-end crashes," *Special investigation report*, 2015.
- [2] J. B. Kenney, "Dedicated short-range communications (DSRC) standards in the United States," *Proc. IEEE*, vol. 99, no. 7, pp. 1162–1182, 2011.
- [3] J. Hatch, A. Topak, R. Schnabel, T. Zwick, R. Weigel, and C. Waldschmidt, "Millimeter-wave technology for automotive radar sensors in the 77 GHz frequency band," *IEEE Trans. Microwave Theory Tech.*, vol. 60, no. 3, pp. 845–860, Mar. 2012.
- [4] A. Bazzi, C. Kärnfelt, A. Péden, T. Chonavel, P. Galaup, and F. Bodereau, "Estimation techniques and simulation platforms for 77 GHz FMCW ACC radars," *Eur. Phys. J. Appl. Phys.*, vol. 2012, no. 57, pp. 1–15, Jan. 2012.
- [5] F. Colone, P. Falcone, C. Bongioanni, and P. Lombardo, "WiFi-based passive bistatic RADAR: data processing schemes and experimental results," *IEEE Trans. Aerospace and Electronic Systems*, vol. 48, no. 2, pp. 1061–1079, Apr. 2012.
- [6] K. Chetty, G. E. Smith, and K. Woodbridge, "Through-the-wall sensing of personnel using passive bistatic WiFi RADAR at standoff distances," *IEEE Trans. Geoscience and Remote Sensing*, vol. 50, no. 4, pp. 1218–1226, Apr. 2012.
- [7] P. Maechler, N. Felber, and H. Kaeslin, "Compressive sensing for WiFi-based passive bistatic RADAR," in *Proc. IEEE European Signal Process. Conf.*, 2012, pp. 1444–1448.
- [8] O. A. K. I. M. Ivashko and A. G. Yarovoy, "Receivers topology optimization of the combined active and WiFi-based passive radar network," in *Proc. IEEE European Radar Conf.*, 2014, pp. 517–520.
- [9] F. Adib and D. Katabi, "See through walls with Wi-Fi!" in *ACM SIGCOMM*, 2013.
- [10] N. Letzepis, A. Grant, P. Alexander, and D. Haley, "Joint estimation of multipath parameters from OFDM signals in mobile channels," in *Proc. IEEE Australian Commun. Theory Workshop*, 2011, pp. 106–111.
- [11] E. R. Yeh, R. C. Daniels, and R. W. Heath, Jr., "Forward collision vehicular RADAR with IEEE 802.11: Feasibility demonstration through measurements," *submitted to IEEE Trans. Veh. Tech.*, 2016.
- [12] C. Sturm, T. Zwick, and W. Wiesbeck, "An OFDM system concept for joint radar and communications operations," in *Proc. IEEE Veh. Technol. Conf.*, Apr. 2009, pp. 1–5.
- [13] C. Sturm, E. Pancera, T. Zwick, and W. Wiesbeck, "A novel approach to ofdm radar processing," in *Proc. IEEE Radar Conf.*, May 2009, pp. 1–4.
- [14] C. Sturm and W. Wiesbeck, "Waveform design and signal processing aspects for fusion of wireless communications and radar sensing," *Proc. IEEE*, vol. 99, no. 7, pp. 1236–1259, Jul. 2011.
- [15] D. Tse and P. Viswanath, *Fundamentals of Wireless Communications*. Cambridge University Press, 2005.
- [16] M. Skolnik, *Introduction to Radar Systems*, 3rd ed. New York: McGraw-Hill, 2002.
- [17] P. Stoica and R. L. Moses, *Spectral Analysis of Signals*. Pearson Prentice Hall, 2005.
- [18] R. Roy and T. Kailath, "ESPRIT-estimation of signal parameters via rotational invariance techniques," *IEEE Trans. Acoust., Speech, Signal Process.*, vol. 37, no. 7, pp. 984–995, Jul. 1989.